Sensitivity enhancement by population transfer in Gd(III) spin labels

Andrin Doll, Mian Qi, Stephan Pribitzer, Nino Wili, Maxim Yulikov, Adelheid Godt, Gunnar Jeschke

Supplementary Information

1. AWG extension

This section describes the connectivity of the AWG to the Bruker Elexsys spectrometer. The formation of monochromatic rectangular microwave pulses in the Elexsys spectrometer is done at X band. In Q-band operation, these pulses are frequency translated using a mixer and a synthesizer. In particular, the carrier frequency of the pulses formed at X band remains fixed at $f_{\text{bridge}} = 9.6453$ GHz, whereas the synthesizer frequency is adjusted to create the desired Q-band frequency. Consequently, the UWB channel was designed to provide shaped X-band pulses at frequencies around f_{bridge} and was connected to the Elexsys spectrometer via a coupler that is otherwise used to inject microwave pulses at a different carrier frequency, the so called *ELDOR* channel. A schematic of this UWB channel is shown in Fig. S.1.

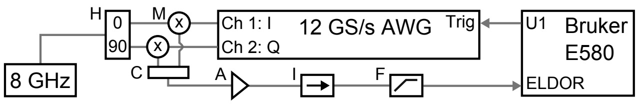

Figure S.1: Schematic of incoherent UWB channel realized by AWG upconversion. H: 90° hybrid, M: Mixer (MITEQ, DM0412LW2), C: Combiner, A: Amplifier (MEURO, MBM0812G2423), I: Isolator, F: Filter (Minicircuits VHF-8400). See text for details.

For the UWB channel, pulse formation was initiated at the AWG upon trigger reception from the Elexsys spectrometer. The pulses synthesized by the AWG satisfied the relation 8 GHz + $f_{\text{AWG}} \in [f_{\text{bridge}} - \Delta f_{\text{bridge}}/2, f_{\text{bridge}} + \Delta f_{\text{bridge}}/2]$, where Δf_{bridge} = 2.5 GHz is the operational bandwidth of the bridge, and had a full scale amplitude of -10 dBm. The frequency translation to X band was by an IQ mixer assembled out of two mixers, a combiner and a 90° hybrid. The microwave carrier for the mixer was 8 GHz (NEXYN, NXPLOS) and an amplifier after the IQ mixer provided the amplitude necessary for insertion into the ELDOR channel. Since there was no fixed phase relation between the microwave pulses from this UWB channel and the microwave carrier of the Elexsys bridge, the UWB channel was incoherent. One can therefore assume that any coherence excited by a shaped pulse from the UWB channel was averaged out in repeated acquisitions.

The primary purpose of this IQ mixer for upconversion is to distinguish between the upper and the lower sideband around the mixer carrier at 8 GHz. In this way, it is possible to generate a microwave pulse in one sideband, with only a residual amount of power directed into the other sideband. This is a crucial capability if the frequencies of the UWB pulse occupy both sidebands. For the experiments presented in this work, this capability turned out to be redundant, because a bandwidth of 2.5 GHz around f_{bridge} for UWB pulses was sufficient. A high pass filter with a cutoff frequency at 8.4 GHz was thus added after the amplifier.

The complications related to pulse distortions mentioned at the end of section 3.2 in the main text are discussed in the next section.

2. Pulse distortions

As mentioned in the main text, *pulse distortions* were one of the limitations for population transfer. This section explains these issues to the hardware-oriented reader. With pulse distortions, we refer to the following situation: Suppose we want to apply a microwave pulse at frequency f_{mw}. Before reaching the spins, this pulse needs to pass the high-power traveling-wave-tube (TWT) amplifier, which is often operated close to saturation. Due to this saturation, the amplified microwave pulse can no longer be described by a perfect cosine function. Typically, there is clipping of the waveform above some amplitude level. In the frequency domain, this leads to higher (odd) harmonics of the input frequency, which is often referred to as harmonic distortion [1]. Consequently, we do not just inject one pulse at a frequency of f_{mw} down to the probehead, but concurrently also some other *spurious pulses* at higher (odd) harmonics. Indeed, these higher harmonics do neither couple well to the spins (resonator bandwidth) nor do they affect the spins in any significant sense (large resonance offset).

The situation is more subtle if a pulse carrying two frequencies $f_{\mathrm{mw},1}$ and $f_{\mathrm{mw},2}$ passes the power amplifier. In this case, the amplified pulse contains a number of (odd) mixing products of $f_{\mathrm{mw},1}$ and $f_{\mathrm{mw},2}$. Prominent output frequencies are the third-order products $2 \cdot f_{\mathrm{mw},1} - f_{\mathrm{mw},2}$ and $2 \cdot f_{\mathrm{mw},2} - f_{\mathrm{mw},1}$. This process is often referred to as intermodulation distortion [1]. As shown in the following example, these combination frequencies can couple well to the spins and lead to resonant excitation.

As explained in the previous section, the observation frequency at Q band translates to a frequency of $f_{\mathrm{bridge}} = 9.6453$ GHz at X band. Since in our experiments the observation frequency was tuned to the maximum of the Gd(III) spectrum as well as the maximum coupling by the resonator, this X-band frequency of $f_{\mathrm{bridge}} = 9.6453$ GHz couples extraordinarily well to the spins. Frequencies below or above f_{bridge} are coupled worse due to the bandwidth of the resonator. If intermodulation (at Q band) was to cause a spurious tone at the (X-band equivalent) frequency f_{bridge}, the effect may turn out rather significant. Assuming that shaped pulses at X band originate from an AWG frequency translated by $f_{\mathrm{LO}} = 8$ GHz using one single mixer, the frequency output by the AWG leads to a pair of frequencies at X band centered around 8 GHz, i.e. $f_{\mathrm{LO}} \pm f_{\mathrm{AWG}}$. Accordingly, a relevant case is when the AWG outputs a frequency of $f_{\mathrm{AWG}} = 0.55$ GHz, hence $f_{\mathrm{mw},1} = 8.55$ GHz, $f_{\mathrm{mw},2} = 7.45$ GHz and $2 \cdot f_{\mathrm{mw},1} - f_{\mathrm{mw},2} \approx f_{\mathrm{bridge}}$. Frequency translation to Q band then results in unwanted excitation at the observation frequency. Note that physically, the frequencies $f_{\mathrm{mw},1}$ and $f_{\mathrm{mw},2}$ are first translated to Q band and only after passing the saturated Q-band amplifier, the spurious frequency appears.

To demonstrate the above case, Fig. S.2a shows the polarization enhancement as a function of the start frequency of the population transfer chirp. The orange curves show up-chirps, with (solid) or without (light) compensation of the resonator bandwidth, whereas the blue curves show down-chirps. In fact, this is exactly the same type of experiment as shown in Fig. 5c, however, obtained with an earlier implementation of the AWG upconverter, which did not use any high-pass filtering or IQ-mixing [2]. Focusing on the orange curves, a rather severe kink is observed at a frequency offset around -1.09 GHz (I). It is at exactly this frequency, where the start frequency of the chirp was at $f_{\mathrm{AWG}} = 0.55$ GHz, thus causing excitation of the observed spins. Below this frequency offset, the spurious chirp pulse due to intermodulation thus passed the observed spins and led to a reduction in polarization by tipping the magnetization. Below this point, another rather pronounced step is observed for an offset around -1.31 GHz (II). Here the start frequency of the chirp was at $f_{\mathrm{AWG}} = 0.33$ GHz, which resulted in a fifth-order product at f_{bridge} ($3 \cdot 8.33$ GHz$-2 \cdot 7.67$ GHz). In summary for the up-chirps, intermodulation distortion leads to spurios chirp pulses at higher frequencies, which eventually tilt the spins to be polarized. The steps observed for the down-chirps have a related, but different origin, and will be addressed further below.

In order to avoid such spurious chirp pulses, microwave pulses injected into the TWT need to have one single instantaneous frequency. For the example above, this can be achieved by canceling the image frequency $f_{\mathrm{LO}} - f_{\mathrm{AWG}}$ by using an IQ mixer or a filter. Here, we give an example with the IQ mixer described in the previous section, but without any filtering. The corresponding polarization enhancements as a function of the start frequency of the chirps are shown in Fig. S.2b. For the

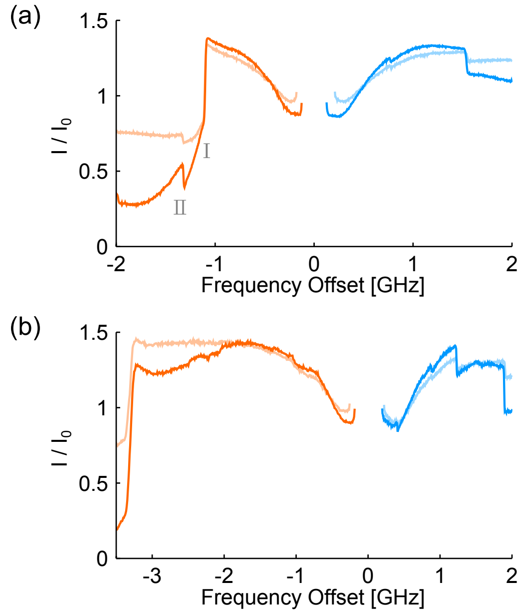

Figure S.2: Unwanted excitation of central line due to spurious frequencies. Both panels show the polarization enhancement as a function of f_1, the start frequency of the chirp, at fixed end frequencies f_2 for up-chirps (orange) and down-chirps (blue) with $t_p = 2\,\mu$s (compare Fig. 4c in main text). The curves with light colors were obtained with constant-rate chirps. (a) Setup with a single mixer for upconversion, without a high-pass filter after the mixer. (b) Setup with IQ mixer for upconversion, without a high-pass filter after the mixer.

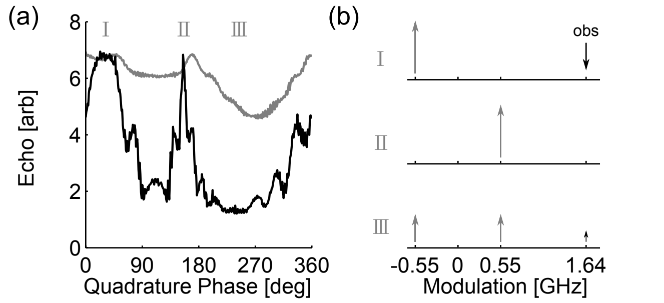

Figure S.3: Cancellation of intermodulation distortion by properly phasing the IQ mixer obtained with (gray) and without (black) high-pass filter. (a) Hahn echo signal as a function of the relative phase at the quadrature output of the AWG. The pulse from the AWG had a length of 100 ns and a constant frequency of $(f_{\text{bridge}} - 8)/3$. The echo signal shows two maxima, I and II. At I, one single frequency in the lower sideband was generated. At II, one single frequency in the upper sideband was generated. For these two cases, the power amplifier sees one single tone at its input. The label III represents an intermediate situation, where the IQ pairs were not in phase quadrature. The power amplifier therefore sees two tones at its input and directs some power into the observation frequency - a process called intermodulation distortion. The corresponding frequency constellations are shown in panel (b). The frequency axis denotes the output frequency of the IQ pair output by the AWG. In this view, the observation frequency f_{bridge} is at 1.6453 GHz.

up-chirp, one readily sees that the steps around -1.09 GHz and -1.31 GHz were no longer observed. A pronounced step can be seen at −3.3 GHz, which corresponds to f_{AWG} = -1.6453 GHz. This step is thus due to imperfections of the IQ mixer, which result in improper cancellation. The IQ mixer was actually calibrated for best cancellation at f_{AWG} = 0.55 GHz and it is not surprising, that imbalance in the IQ mixer would require a different calibration at a 2 GHz frequency offset. The calibration procedure at f_{AWG} = 0.55 GHz is outlined in Fig. S.3 and was performed by minimizing the impact of the intermodulation tone onto the observed spins (see caption for description).

For the steps in polarization enhancement observed with down-chirps, a related effect took place. With frequencies above the observed spins, the intermodulation process described for the up-chirps does not apply here. However, the upconversion mixer itself may create spurious chirp pulses by higher-order mixing products: While a single mixer primarily outputs first order products at $f_{\text{LO}} \pm f_{\text{AWG}}$, mixing products of higher order may also occur. Using a spectrum analyzer and test tones from the AWG at strategical frequencies, the steps observed for the down-chirps in Fig. S.2b have been assigned to such mixing products. The solution to minimize such products is rather straightforward: Reduction of the drive level of the AWG at the mixer, which resulted in the −10 dBm full scale amplitude used in the main text. A lower drive level results in lower power microwave pulses, which requires a different power leveling after the mixer. Furthermore, the relative strength of carrier leakage at f_{LO} increases towards smaller drive levels.

Since present experiments did not require the bandwidth provided by the IQ mixer, a high-pass filter was installed, as described in the previous section. As a side effect, this filter also reduced the carrier leakage. The filter in principle renders the IQ mixer redundant in terms of excitation bandwidth. However, we could still observe an effect of the phase on the IQ mixer at f_{AWG} = 0.55 GHz (see gray in Fig. S.3). The rejection of the image at 7.45 GHz by the high-pass filter was therefore not sufficient with respect to third order intermodulation. For upconversion setups using a single mixer combined with a filter instead of the IQ mixer, this needs to be taken in consideration. The upconversion arm described in [3] is such a single mixer setup with a filter. There, however, the operational bandwidth was from 8.75 GHz to 9.5 GHz, thus not including the critical 8.55 GHz frequency (see also SI of [3]).

At the current stage, the spurious intermodulation chirps are reduced to a negligible level. However, if sample heating would not inhibit the use of longer pulses with larger bandwidths, such problems might again become important. A general aspect of these spurious chirps is that their impact is only significant at the center of the resonator. Off the center, the adiabaticity of these spurious chirps is reduced by a fair amount. Furthermore, a spurious chirp at the center of the resonator implies that the intended chirp pulse couples weakly to the spins, as it is off the center (for single mode resonators). Since we use pulses which compensate for the coupling to the spins, the chirp pulse slows down its sweep rate towards the weaker coupling off the center [2]. As a consequence, the spurious chirp has a slowed down sweep rate when passing the center of the resonator, which compensates for its low power and results in an enhanced adiabaticity. This is actually the reason, why all of the steps in Fig. S.2 are larger for the compensated pulses than for the non-compensated pulses.

(Text continues on next page)

We may add that for the excitation power of the spectrometer at bandwidths around 300 MHz, representative values for π pulses on $S = 1/2$ spins are on the order of 12 to 14 ns, which corresponds to π pulses on the central line of Gd(III) in the range of 3 to 3.5 ns. The longer pulse lengths on the CT on the order of 4.5 ns related to the experiments in the main text were due to a temporary replacement power amplifier. In fact, this temporary replacement showed an unexpected spurious response that reduced the efficiency for down-chirps. To circumvent this specific response, the drive level on the amplifier was reduced by reducing the AWG drive level from −4 dBm to −10 dBm, thus prolonging the pulse length (see the corresponding reduction factor of 75% at the end of section 3.2 in the main text). It was presumed that the larger input bandwidth of the replacement amplifier caused these extra spurious frequencies to appear, but a Q-band filter to test this assumption was not available.
As a reference, the spurious response with a drive level of −4 dBm is shown in Fig. S.4. These data were taken with the UWB channel shown in Fig. S.1, however, with the proper power amplifier allowing for operation at a −4 dBm drive level from the AWG. In order to ease the identification of spurious tones, an ELDOR hole-burning type experiment was performed. The effect of a monochromatic high-turning angle (HTA) pulse with frequency varied over a range of 4 GHz was probed by Hahn echo observation at the center of the resonator/Gd(III) spectrum. Curve (a) was obtained with a 100 ns long HTA pulse. Before the pulse overlapped at the center, the echo intensity was enhanced by a few percent due to population transfer from its immediate neighbor transitions. In addition, there were two distinct peaks at offsets beyond 1.5 GHz, which correspond to spurious tones exciting the observed spins. The most pronounced one at an offset of 1.766 GHz was actually also observed as a small step when setting up the population transfer.
For curve (b), the pulse length was increased to 1 μs. Population transfer could no longer be observed, but additional spurious tones of smaller amplitude appeared. At a frequency offset of −0.822 GHz, the second harmonic of the AWG output excited the observed spins. Inspection of the X-band pulses from the UWB channel with a spectrum analyzer revealed that this second harmonic distortion led to a spurious signal at f_{bridge} with a level 44 dB below the full-scale level. When setting up the population transfer experiment, this second harmonic spurious did not lead to an observable step. A 1 μs monochromatic pulse concentrates way more power at a given frequency than an UWB chirp pulse with twice the pulse length.
Curve (c) was obtained with a miscalibrated quadrature phase. As was already observed for a 100 ns pulse (see gray in Fig. S.3), there was third-order intermodulation despite the high-pass filter for image rejection. In curve (d), the entire spurious response was stimulated by doubling the drive amplitude at the AWG to 2 dBm. All the lines marked with a black star are formally harmonics of the AWG output frequency f_{AWG}. From the even harmonics, only the second and fourth harmonics could be detected, whereas for the odd harmonics, the highest one was the ninth harmonic. The lines marked with a green star are mixing products, which formally depend on f_{AWG} and the translation frequency $f_{\mathrm{LO}} = 8$ GHz.

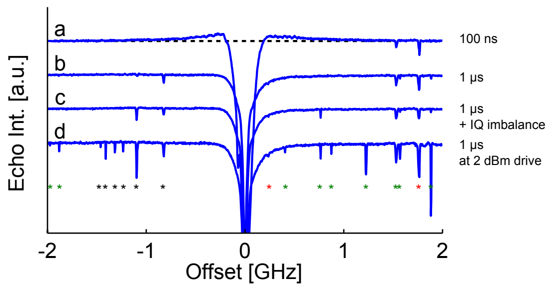

Figure S.4: Spurious response probed by hole burning experiment using a monochromatic high-turning angle (HTA) pulse over an offset range of 4 GHz. All curves were normalized to an intensity of 1 and vertically displaced by 0.15. The 100 ns HTA pulses were sinusoidally smoothened during 10 ns, the 1 μs were smoothened during 250 ns. All HTA pulses were at maximum power. (a) 100 ns HTA pulse showing two higher order spurs as well as population transfer, exclusively from neighbor transitions. (b) 1 μs long HTA pulse showing a spur at an offset of $-1.6453/2$, thus a second harmonic of the frequency f_{AWG} ouput by the AWG. (c) 1 μs long HTA pulse with quadrature phase offset by 30°, which shows additional spurs. At an offset of $-1.6453 \cdot 2/3$ for instance, a third order intermodulation spur is detected. (d) 1 μs long HTA pulse at 2 dBm drive level, which uncovers a number of spurious frequencies. The ones marked with a black star do formally only depend on the AWG output frequency f_{AWG}. The ones with a green star are mixing products between f_{AWG} and the translation frequency $f_{\mathrm{LO}} = 8$ GHz. The two spurs with a red star were not assigned, since these depended on other frequencies.

All the frequencies marked in green or black give rise to a tone at $f_{\mathrm{bridge}} = 9.6453$ GHz, which was verified experimentally by inspection of the X-band pulses from the UWB channel with a spectrum analyzer. However, there are two frequencies marked with a red star. These cannot be assigned as mixing products of f_{AWG} and f_{LO}, and these were also not detected with a spectrum analyzer at X-band. In particular, the rather pronounced peak at 1.766 GHz does depend on the frequency translation from X to Q band inside the Bruker spectrometer: A change in the Q-band observation frequency moved the position of this peak. Such a behavior was not observed for the other tones labeled in green and black. Since this spurious frequency at 1.766 GHz emerged as a small step in setting up the down-chirp for population transfer, this frequency could become important for down-chirps of longer duration with optimized start frequencies beyond this 1.766 GHz frequency offset.

3. Sample heating

Due to the long chirp pulses, sample heating effects were observed. The most direct approach to such effects is observation of the intensity of the Hahn echo upon pre-polarization pulses, as shown in Fig. S.5a. The orange and blue curves show the polarization enhancement as a function of time for the up-chirp and down-chirp optimized in section 3.1 in the main text. The solid green curve was obtained by sequentially combining the two pulses, whereas the dashed green curve was obtained with two optimized pulses with half the pulse length (1 μs).
Before each of these measurements, the sample was in thermal equilibrium. Once the pre-polarization pulses were switched on at time $t = 0$, one would expect the pre-polarized signal to remain constant at all times. The actual data, however, showed decaying polarization. When comparing the up-chirp to the down-chirp, the decay upon the up-chirp was more pronounced. This pronounced decay shape also appeared for the sequentially combined pulses. Consequently, the up-chirp induced this unexpected behavior.
For an estimate of the sample heating, we measured the echo intensity at various temperatures (Fig. S.5b) and observed a decay of roughly 9% per K. The local heating due to the up-chirp was thus on the order of 1 K. With the shorter 1 μs pulses combined together, heating effects were less pronounced. Nevertheless, the net enhancement with the shorter pulses remained smaller than for the combined 2 μs pulses. Notably, we could observe back-action from this local heating to the temperature reading of the regulation system (Oxford CF935). This effect has been suppressed by using sufficient under-pressure above 200 mbar to the cryostat.
This sample heating is one reason for not increasing the pulse length in order to obtain larger signal enhancements. At least with our experimental setup, the pulse length was restricted by technical limitations and not by relaxation characteristics of the sample. Since only the up-chirp at negative frequency offsets led to significant heating, a heating mechanism specific to the utilized resonator is presumed. In fact, the resonator employs oversized sample tubes for a larger filling factor [4, 5], which may in turn increase possible heating by the electric field.
Because the unstable baseline due to the heating is undesirable in almost all measurements, approaches towards a more stable baseline have been tested. Sufficient stabilization for distance measurements reported in section 3.3 in the main text was achieved by means of (i) *pre-heating* the sample with pulses prior to acquisition and (ii) adaptation of the time for each scan (increase in shots per point). Further information is found in Fig. S.6 below. In all other experiments in the main text, such as the pulse calibration experiments described in section 3.1 or the field-sweeps in section 3.2, no particular stabilization of the baseline was implemented.
Considering the polarization enhancements at $t = 0$, each of the 2 μs long pulses led to roughly 70% stronger signals. The simulation in section 2.2 in the main text actually showed an enhancement of 78%. Despite a number of approximations involved in this particular powder simulation (see section 2.4 and Fig. S.13a), the described procedure seems to be an appropriate starting point for further refinements. For the sequential combination of these two pulses at $t = 0$, one may expect twice the experimental enhancement of 70%. However, the experimental enhancement was 114%. Understanding the origin of this reduced experimental enhancement with combined pulses requires further investigation. A partial contribution to this reduction was an apparently longer equilibration time with the combined pulses (see Fig. S.7 below). At present, the most important aspect is the significant increase of experimental enhancements with the combined pulses.

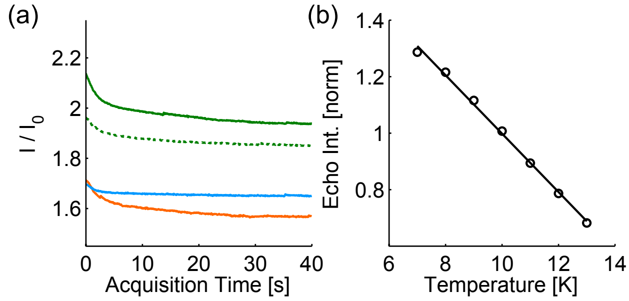

Figure S.5: Sample heating due to pre-polarization chirps. (a) Time dependence of the intensity of the pre-polarized central line for 2 μs long up-chirp (orange), down-chirp (blue) and sequential combination of both (solid green). All chirps with optimized positioning as depicted in Fig 4c in the main text. The dashed green line was obtained with two sequentially combined 1 μs chirps (f_1 = -1.14 GHz to f_2 = -0.124 GHz and f_1 = 1.062 GHz to f_2 = 0.142 GHz). (b) Experimental equilibrium polarization versus temperature (black circles) and linear fit with a descent of 9% per K. Note that the repetition time was kept constant, such that the values at lower temperatures were reduced by saturation.

3.1. *Heating transients*

In this section, the heating transients due to the up-chirp are shown in more detail. The black curve in Fig. S.6a corresponds to the green curve in Fig. S.5, but acquired for a longer time. As can be seen, it took almost 1 minute to fully equilibrate to the new conditions brought by the chirp pulse. The way around this long equilibration time was by pre-heating the sample, which we performed for 34 seconds, as indicated by the arrow. The resulting transient (gray) was much shorter. The pre-heating was readily implemented as a loop with a predefined number of repetitions of the pulse sequence, but without any actual acquisition command. Upon the termination of this loop, the main acquisition loop started, which led to a reprogramming timeout on the order of 1 second. It is presumed that it is thermalization during this delay, which caused the remaining transient observed with pre-heating. We would expect this transient to become even shorter and less pronounced for faster reprogramming times. We observed this kind of delays also after each completed average in the main acquisition loop, however, not during the loop, since phase cycling can be performed without any reprogramming delays.
With the shorter transient upon pre-heating, the number of shots per point was adjusted to concentrate this transient only in the

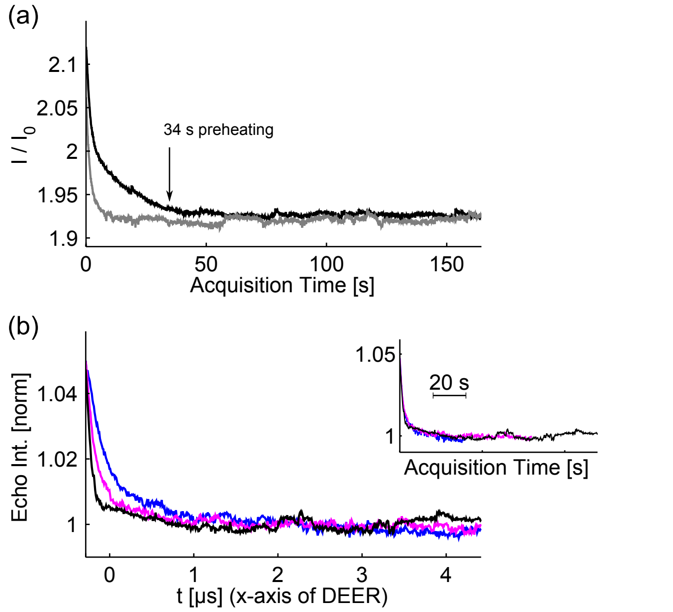

Figure S.6: Pre-heating to reduce transients at the beginning of experiments. (a) Time dependence of the pre-polarized central line intensity (double-sided pre-polarization) for extended acquisition time, as compared to the Fig S.5. The black curve was obtained without pre-heating. The gray curve was obtained with pre-heating for 34 seconds, as indicated by the black arrow. The transient with the long time-constant could be reduced with the pre-heating. A faster transient at the beginning remained. This originated from thermalization during the reprogramming-timeout in between scans, which is on the order of 1 s. (b) Shortening of the remaining fast transient with pre-heating by changing the shots per point: 200 shots (blue), 400 shots (magenta), 600 shots (black). The x-axis is indicated as the time axis that would result for a DEER experiment. The inset shows the same data as a function of acquisition time. Some residual slow transient can be identified, because the three curves show a similar trend.

first few points of a 1D experiment. Indeed, the four-pulse DEER sequence is an especially generous case, since the first few points are anyhow not used in the data analysis. Fig. S.6b thus shows the baseline of the pre-polarized DEER experiment in the absence of the pump pulse using 200 (blue), 400 (magenta) or 600 (black) shots per point. For the black curve, the transient has decayed sufficiently before the DEER signal started at $t = 0$. The baseline fluctuations starting from $t = 0$ were on the order of 0.5%. The inset on the right hand side furthermore shows the three curves as a function of acquisition time. In the overlay, all curves reveal a residual slow decay after the initial steep descent. It is presumed that this decay resulted from too short pre-heating time. In the actual pre-polarized DEER experiment, however, the second average of the scan is effectively pre-heated for a longer time period due to the previous scan. Accordingly, one would expect this slower transient to vanish in averaged data. Nevertheless, pre-heating of the very first scan turned out to be always advantageous, since the transient of the first scan was otherwise too extended. At reduced concentrations and extended dipolar evolution times, heating transients may become comparable to the noise level, so that pre-heating can be largely neglected when using a sufficient number of shots per point.

4. Relaxation effects

4.1. Saturation effects for double-sided transfer

As discussed above at the end of section 3 in this ESI, the combined enhancement with two chirp pulses was not the sum of the enhancements achieved with one single chirp. The two single pulses led to an enhancement of 70%, whereas the combined enhancement was 114%. It was found that the combined enhancement had a different dependence on the repetition time of the experiment.

Fig. S.7a shows intensities of the pre-polarized central line for various repetition times. Pre-polarization was either by up-chirps (orange), down-chirps (blue), or the sequential combination (green open circles). Influences of heating were minimized by measuring these intensities shortly after starting the experiment. Ten shots at the beginning were skipped to avoid apparent contributions from saturation at fast repetition times. The expected intensities obtained by summing the enhancements from the up-chirp and the down-chirp are indicated by the green triangles. As is seen in this representation, the shot repetition time had a weaker influence on the data obtained with a single chirp pulse than on the data obtained with the combined pulses.

Fig. S.7b shows the loss factor, which is the experimental intensity with the combined chirps (green circles in panel a) divided by the expected intensity (green triangles in panel a). This factor increases for longer repetition times to a maximum of roughly 93%. The different behavior of the double-sided enhancement suggests different equilibration dynamics. For fur-

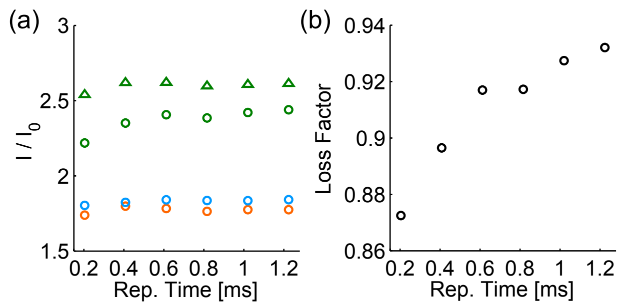

Figure S.7: Dependence of the intensity of the pre-polarized central line on the repetition time of the experiment. The up-chirp had optimized frequencies $f_1 = -1.46$ GHz and $f_2 = -0.18$ GHz. The down-chirp had $f_1 = 1.5$ GHz and $f_2 = 0.154$ GHz. (a) Experimental intensity upon up-chirp (orange), down-chirp (blue), and sequential combination (green open circles). The intensities were extracted just after turning on the pre-polarization pulses to minimize heating contributions. For each data point, the equilibrium intensity I_0 for normalization was obtained using the corresponding repetition time. The green triangles represent the intensity one would expect from summing the experimental up-chirp and down-chirp enhancements. (b) Loss factor obtained by dividing the experimental combined intensity (green circles in a) by the expected intensities (green triangles in a).

ther investigation, simulations of the multi-level dynamics are required.

4.2. Loss of enhancement with prolonged evolution times

In this section, echo-detected field-sweep spectra of Gd-spacer-Gd **1** were recorded with inter-pulse delay between observation pulses prolonged to 7 μs. This inter-pulse delay mimics the long evolution times of coherence on Gd(III) transitions that is typical for DEER experiments. The equilibrium spectrum obtained in this way is illustrated by the solid black curve in Fig. S.8a. As compared to the spectrum recorded under ordinary conditions (dashed black), the shoulders of the spectrum were largely attenuated by transverse relaxation. With pre-polarization from both sides, the spectrum indicated by the green curve was obtained. The range, over which the pre-polarized signal is stronger than the peak equilibrium signal, was here reduced from 16 mT to 9 mT. The normalized intensities I/I_0 for this case are shown in Fig. S.8b. The solid curves show the data for up-chirp (orange), down-chirp (blue) and the combination (green), whereas the dashed green curve shows the data for the combination under ordinary conditions from Fig. 5b in the main text.

Interestingly, the polarization enhancement with the prolonged pulse delay already dropped to 0 beyond ±50 mT. The transitions beyond these points could thus no longer be observed with this scheme. In general, the solid green curve appears vertically offset from the dashed green curve, which indicates that some transitions did no longer contribute to the observed signal. Only at the central line, whose FWHM is indicated by the dashed black lines, the vertical offset is negligible, because the relative contribution of satellite transitions is rather small there. Outside the central line, this vertical offset was on the order of 15% of the dashed green curve.

The reduction to zero enhancement at ±50 mT actually indicates that only inversion of the CT results in detectable polarization enhancement. Beyond ±50 mT, the CT does no longer contribute and population is only transferred within satellite transitions (see main text). For the data obtained with 7 μs inter-pulse delay, it is thus reasonable to assume that out of all satellites, exclusively the $\pm 3/2 \leftrightarrow \pm 1/2$ transitions contributed to the observed signal.

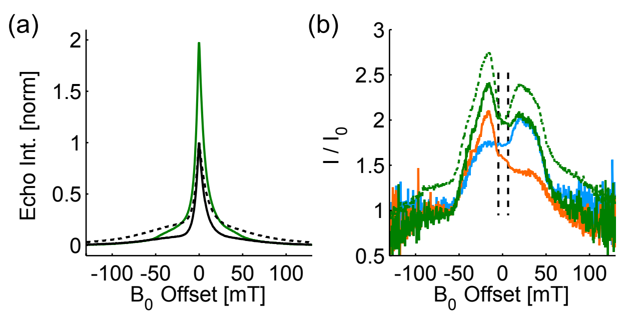

Figure S.8: Pre-polarized field-swept spectra with inter-pulse delay prolonged to 7 μs. (a) Field-sweep obtained with sequentially combined chirps (green) and without pre-polarization (solid black). The dashed black curve represents the equilibrium reference from Fig 5a in the main text. (b) Field dependence of polarization obtained with up-chirp (orange), down-chirp (blue) and sequential combination of both (solid green). The dashed green curve represents the corresponding curve from Fig 5b in the main text. The dashed black vertical lines indicate the FWHM of the central line.

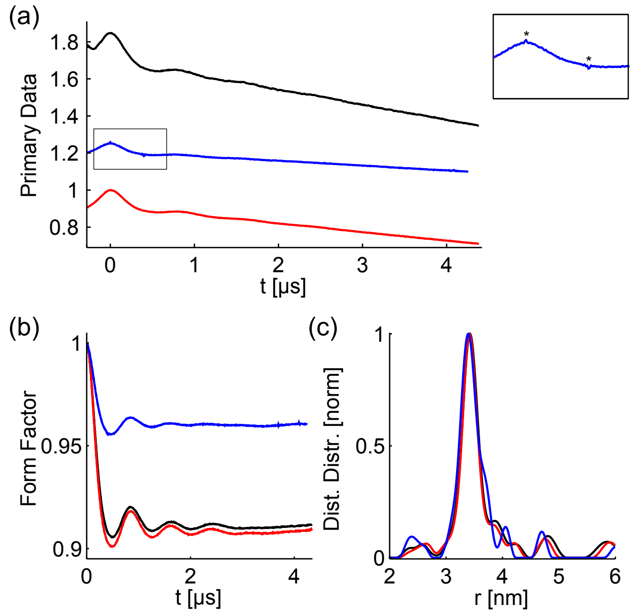

Figure S.9: Pre-polarized DEER experiments on Gd-spacer-Gd **1** using a 192 ns long chirp pump pulse (compare Fig. 7 in main text) and reference experiment with a rectangular 9 ns pump pulse at −0.3 GHz. (a) Primary data obtained with pre-polarization to 1.85 (black), without pre-polarization (red) and with rectangular pulse (blue). Ordinate normalized to echo signal of red curve. The echo signal with the rectangular pump is 1.25. The inset shows a zoom on the rectangular pump data and reveals two artificial spikes marked with *. These originate from coherence excited by the pump and refocused by the observer pulses, thus an effect of spectral overlap between pump and observer. (b) Form factors with (black) and without (red) pre-polarization showing modulation depths on the order of 9% and form factor for rectangular pulse (blue) with modulation depth of 4%. The two spikes visible at the end of the blue curve are of the same origin as those highlighted in the inset above. (c) Regularized distance distributions with (black) and without (red) pre-polarization and rectangular pulse (blue).

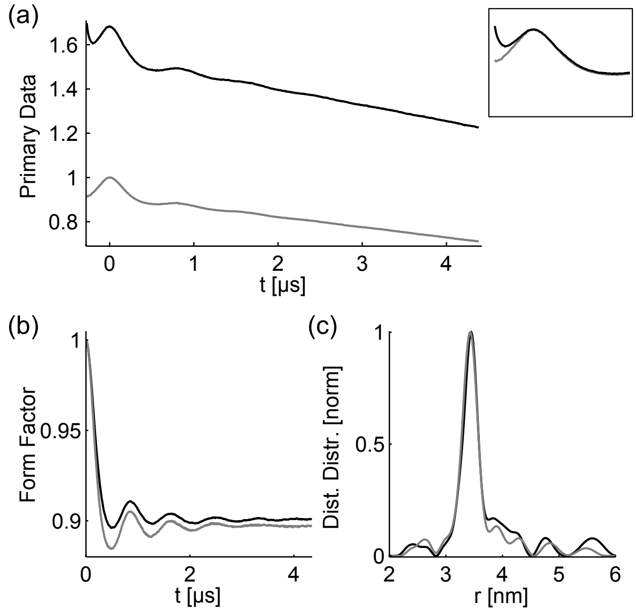

Figure S.10: Pre-polarized DEER experiments on Gd-spacer-Gd **1** with a Gd-Gd distance of about 3.4 nm using a 192 ns long chirp pump pulse (f_1 = -0.875 GHz to f_2 = -0.3 GHz, adiabaticity on CT of 2.24). The 2 μs pre-polarization pulses had ranges f_1 = -1.396 GHz to f_2 = -0.092 GHz and f_1 = 1.286 GHz to f_2 = 0.150 GHz. (a) Primary data obtained with pre-polarization to 1.68 (black) and without pre-polarization (gray). The inset on the right-hand side shows the initial part of the two curves on top of each other. The pre-polarization was only 1.68 due to erroneous programming of chirp start frequencies f_1. The correct optima would be f_1 = -1.228 GHz and f_1 = 1.07 GHz. (b) Form factors with (black) and without (gray) pre-polarization showing modulation depths of 10%. (c) Regularized distance distributions with (black) and without (gray) pre-polarization.

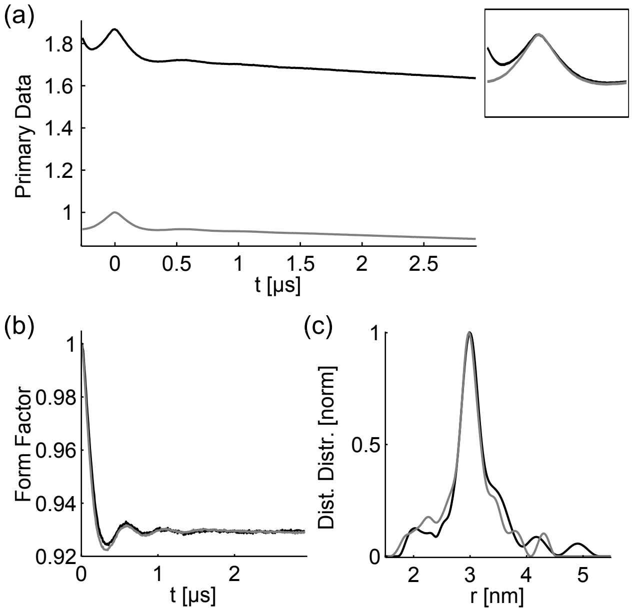

Figure S.11: Pre-polarized DEER experiments on Gd-spacer-Gd **2** with a Gd-Gd distance of about 3.0 nm using a 64 ns long constant-rate chirp pump pulse (f_1 = -0.75 GHz to f_2 = -0.3 GHz). The 2 μs pre-polarization pulses had ranges f_1 = -1.273 GHz to f_2 = -0.121 GHz and f_1 = 1.349 GHz to f_2 = 0.133 GHz. (a) Primary data obtained with pre-polarization to 1.86 (black) and without pre-polarization (gray). The inset on the right-hand side shows the initial part of the two curves on top of each other. (b) Form factors with (black) and without (gray) pre-polarization showing modulation depths of 7%. (c) Regularized distance distributions with (black) and without (gray) pre-polarization.

5. Pre-polarized distance measurements

In the following, supplementary DEER data are presented. First of all, all the data from Fig. 7 in the main text are shown in Fig. S.9, where the data without pre-polarization are shown in red and the data with pre-polarization are shown in black. In addition, the reference experiment obtained with a 9 ns long monochromatic rectangular pump pulse at a frequency offset of -0.3 GHz is shown in blue, which is an experimental scheme according to [6]. This experiment resulted in a 25% larger echo signal, but only 4% modulation depth. This led to the enhancement factor of 1.8 by using an optimized chirp pump pulse instead of a monochromatic pump pulse. Combining this enhancement with the signal enhancement by pre-polarization, a net enhancement factor of 3.33 was obtained. The distance distributions obtained with the chirp pump pulse and with the monochromatic pump pulse showed reasonable agreement.

Besides this monochromatic pump pulse, pre-polarized DEER data from two other experiments are presented. In Fig. S.10, essentially the same experiment on Gd-spacer-Gd **1** as the one in the main text is shown. These data confirm again that distance distributions overlay quite well, independent on whether pre-polarization was used or not. The only problem with these data is the lower polarization enhancement of 68%, which was due to erroneous programming of the chirp start frequencies after the optimization. The modulation depth was roughly 10%.

Another dataset is presented in Fig. S.11. Here, Gd-spacer-Gd **2** with a distance of roughly 3.0 nm between the two Gd(III) ions was used (see section 3.1.1 and [7]). Pre-polarization resulted in an enhancement of 86% and the modulation depth was 7%. As can be recognized by comparing the heating transient in the on the top right with equivalent insets in Fig. S.10 and 9, the transient was somewhat longer due to acquisition with only 200 shots per point. The resulting distance distributions showed reasonable agreement.

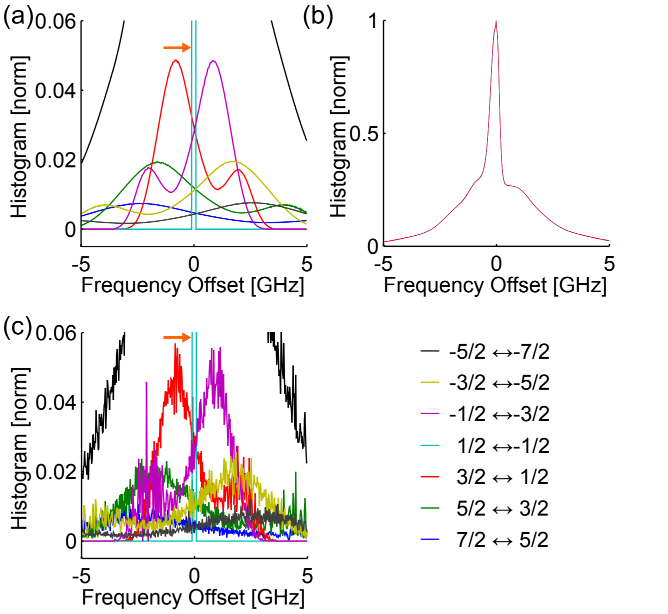

Figure S.12: Supplementary Gd(III) spectra from powder simulations. See main text for simulation method. (a) Histogram of single-quantum transition frequencies of $\hat{\mathcal{H}}_{\mathrm{ZFS}}$ (black) obtained with perturbation theory for frequency offsets of ± 5 GHz with 24 MHz step size. A zoom on the satellite transitions of the simulation subset is shown, according to the color legend on the bottom right. The grid for averaging over D, E, θ and ϕ consisted of 90 points in each dimension, thus much finer than in the main text (1000x more configurations). The spectrum calculation required 2.2 minutes. The orange arrow indicates the frequency range of the chirp pulse from -1.348 GHz to -0.124 GHz. (b) The ZFS spectrum of all single-quantum using the fine grid of (a) obtained with perturbation theory (red) as well spectrum calculated with eigenvalues of the full Hamiltonian and transformation of $\hat{S}_x$ into the eigenframe for transition moments (blue). (c) Same data as in (a), but for the grid used in the spin dynamics simulation in the main text.

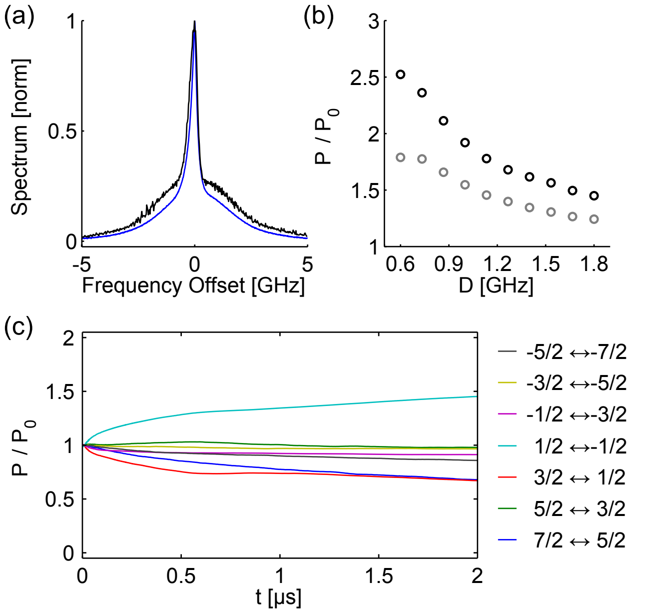

Figure S.13: Powder simulation of chirp with inverted direction. (a) Histogram of powder simulations with μ_D = 1.2 GHz and σ_D = 0.24 GHz (black) compared to experimental echo-detected field-swept spectrum of Gd-spacer-Gd **1** connected to a frequency axis. Note that the simulated spectrum assumes only Zeeman and ZFS contributions in the high-temperature limit. (b) Simulated polarization of the powder- and E-averaged subset of the CT upon the chirp pulse at various D values. The black dots are the ones from the main text. The gray dots were simulated with the same parameters, just that the direction of the chirp was inverted. In this way, the CT can only be polarized via one of its neighbor transitions. (c) Simulated evolution of powder- and ZFS-averaged polarization under the chirp with inverted direction for the simulation subset. Color legend on the right-hand side. For the CT, the polarization upon the pulse is 1.48, which corresponds to the weighted average of polarizations in panel (b). This polarization is lower than the one simulated in the main text by 0.3. As a consequence for the simulation in the main text, 38% of the population transferred to the CT origins from transitions beyond the immediate neighbors.

6. Supplementary simulations

In this final section, supplementary simulations are presented. At first, Fig. S.12 shows the simulation subset in Fig. 2a of the main text. In Fig. S.12a, a zoom on the satellite transitions is shown. The grid for computing the spectrum consisted of 90 points for all involved parameters, such that smoother histograms were obtained. Fig. S.12b shows the sum of all single-quantum transitions on this fine parameter grid. The red curve was calculated with perturbation theory, whereas the blue curve (underneath the red curve) was obtained by diagonalization of the laboratory frame Hamiltonian. For the given parameter grid, the two methods resulted in almost indistinguishable results. Needless to add, the diagonalization in the laboratory frame on this grid required more computation time. Moreover, our simulation approach does not support non-diagonal Hamiltonians with spectrum beyond the Nyquist range of 6 GHz due to the time stepping in the rotating frame. The perturbation approach was thus essential. Fig. S.12c shows the same view as in panel a, but with the coarser grid used in the actual spin dynamics simulations.

Fig. S.13a relates the powder simulations with a Gaussian distribution of D values (μ_D = 1.2 GHz and σ_D = 0.24 GHz) (black) to the echo-detected spectrum of Gd-PyMTA of Gd-spacer-Gd **1** (blue). Note that at present, simulated spectra assume the high-temperature limit and that all transitions are observed with the same efficiency. For the experimental data, however, the echo-detection introduces additional transition-specific weightings and the high-temperature limit is not strictly valid. Neglecting ZFS contributions, the equilibrium polarizations for an S = 7/2 system at 10 K and 35 GHz are already non-equal: The central transition carries only 60% of the polarization of the lowest transition, the highest transition even only 37%. Inclusion of such effects into the simulation may help to refine parameter grids for better fits between experiment and simulation. For the present purpose, however, the simulations served to confirm the experimental trends with respect to different Gd(III) complexes.

Fig. S.13b shows the same black circles as Fig. 2b in the main text, which correspond to polarization upon the chirp for the various D values. The gray open circles were obtained with a chirp having inverted sweep direction, thus only polarizing the CT via one immediate neighbor transition. Due to the exclusion of polarization from satellites further out, the achieved polarizations were all lower than for the up-chirp simulated in the main text. This simulation was performed to support the conclusions drawn in section 4.1.1. The underlying dynamics of polarization averaged over all involved D values is shown in panel c. The last figure, Fig. S.14, shows evolution of polarization during the up-chirp of the main text for a set of the individual D values, as indicated in each plot.

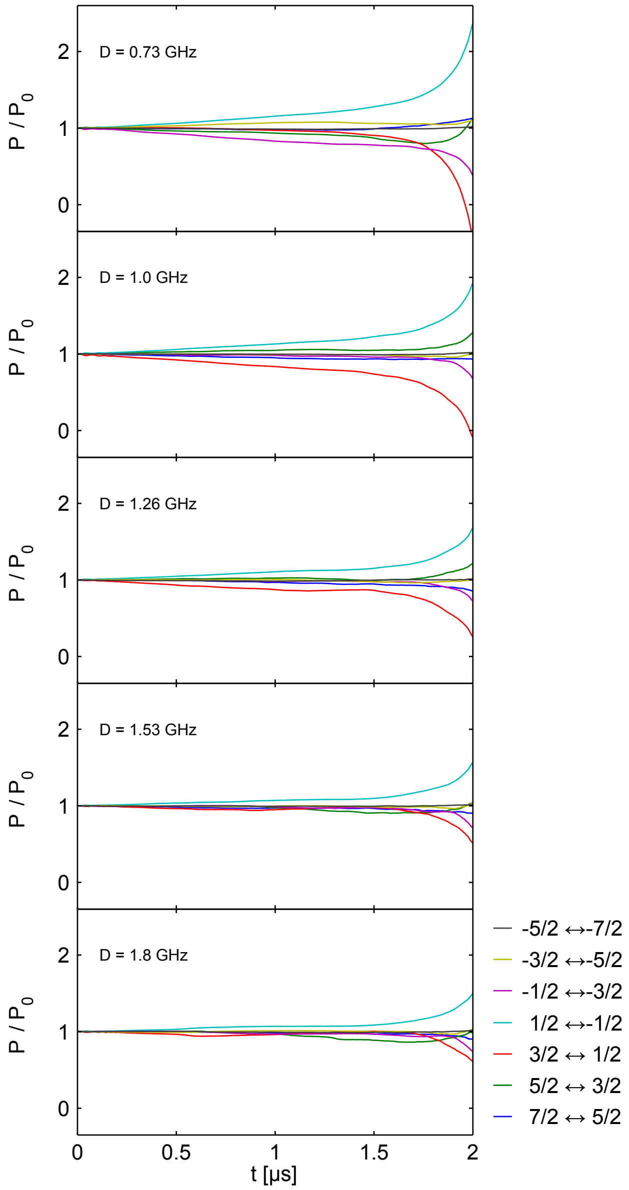

Figure S.14: Evolution of polarizations averaged over orientation and E distribution within simulation subset (see main text) for 5 different D values, as indicated on each figure. Color legend on bottom right

References

[1] D. Pozar, *Microwave Engineering*, 4th edn.

[2] A. Doll, S. Pribitzer, R. Tschaggelar and G. Jeschke, *J. Magn. Reson.*, 2013, **230**, 27 – 39.

[3] A. Doll and G. Jeschke, *J. Magn. Reson.*, 2014, **246**, 18 – 26.

[4] R. Tschaggelar, B. Kasumaj, M. G. Santangelo, J. Forrer, P. Leger, H. Dube, F. Diederich, J. Harmer, R. Schuhmann, I. Garca-Rubio and G. Jeschke, *J. Magn. Reson.*, 2009, **200**, 81 – 87.

[5] Y. Polyhach, E. Bordignon, R. Tschaggelar, S. Gandra, A. Godt and G. Jeschke, *Phys. Chem. Chem. Phys.*, 2012, **14**, 10762–10773.

[6] A. Raitsimring, A. Astashkin, J. Enemark, I. Kaminker, D. Goldfarb, E. Walter, Y. Song and T. Meade, *Appl. Magn. Reson.*, 2013, **44**, 649–670.

[7] M. Qi, A. Groß, G. Jeschke, A. Godt and M. Drescher, *J. Am. Chem. Soc.*, 2014, **136**, 15366–15378.